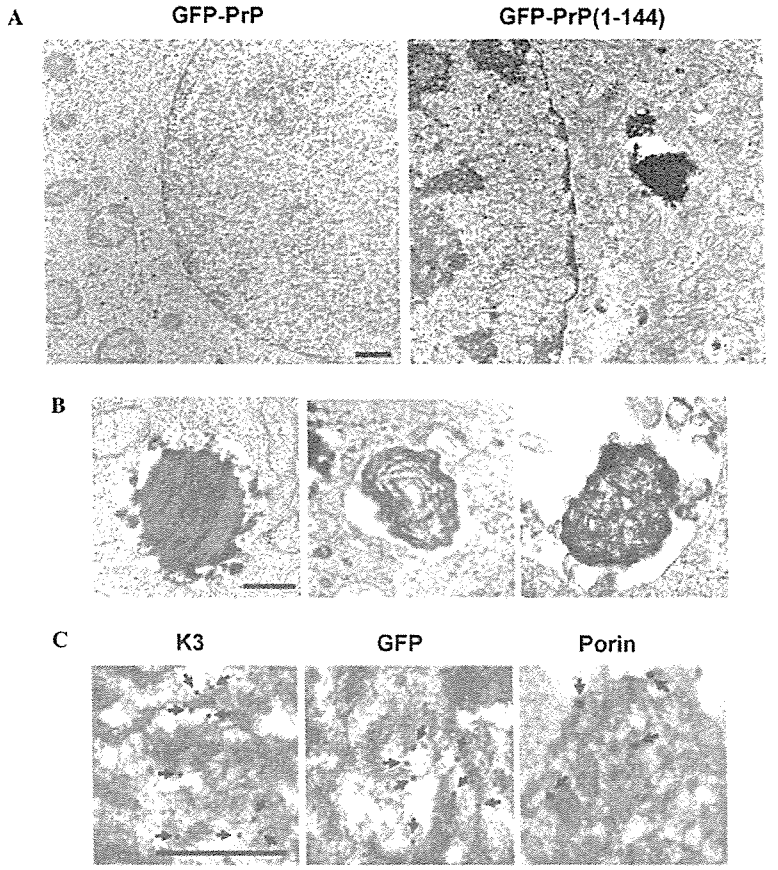


Fig. 3. GFP-PrP(1–144)-related electron-dense deposits. Scale bars = 0.1 μm. (A) Electron microscopy (30,000×) detects numerous electron-dense deposits in N2a cells transfected with GFP-PrP(1–144), whereas full-length GFP-PrP induces no deposit. (B) Some vesicles contain myelin-like figures. (C) Immunoelectron microscopy (30,000×) detects GFP-PrP(1–144) with anti-PrP antibody K3 (10 nm golds, left panel) or anti-GFP antibody (10 nm golds, middle panel) within the electron dense deposits of N2a cells. Anti-porin antibody (20 nm golds) also stains the deposits (right panel).

chondria-mediated apoptosis. Consequently, such neurotoxic property may contribute to a common pathogenic mechanism shared in various PrP-related disorders.

Deposition of numerous electron-dense deposits immunostained with anti-PrP antibody is another characteristic in GFP-PrP(1–144)-transfected cells, and has not been reported in other studies so far. The relevance of such electron-dense deposits with PrP amyloid deposits, a characteristic feature of human GSS with Y145STOP, is an intriguing question. These amyloid plaques were composed of COOH-terminal truncated PrP [12], but have not transmitted to mice [17]. Of note, both the electron-dense deposits in Y145STOP-transfected N2a cells and $PrP^{Sc}$ in scrapie-infected N2a cells were found in the similar vacuolar compartment resembling secondary lysosomes [23], suggesting that both deposits may share a similar resistance to such a harsh lysosomal condition.

The Y145STOP mutation has been widely investigated in terms of its biochemical property. Peptides encompassing PrP(89–143) when mixed with $PrP^{C}$ produced fibrous aggregates and displayed a high β-sheet content, although no prion infectivity was observed [24,25]. Recently, Kundu et al. [26] reported a spontaneous conversion of the recombinant polypeptide, human PrP(23–144), from a monomeric unordered state to a fibrillar form, in which human PrP residues within the 138–141 region are essential. Interestingly, this conversion has characteristics of a nucleation-dependent polymerization. Whether the numerous electron-dense deposits may serve as a seed for the growth of amyloid plaques with Y145STOP awaits further investigations.

Our current observations may provide clues as to the yet unknown underlying mechanism concerning the heritable human prion disease with Y145STOP at least in part. At the same time, the prion disease with Y145STOP has untransmitted to mice [17]. How this relates to the puzzle in prion biology, the discrepancy between the infectious and neurotoxic properties of PrP [27], remains to be further examined.

## Acknowledgments

We greatly thank T. Onodera for providing the HpL3-4 cell line, E. Nannri, K. Ishibashi, C. Ota, and S. Wajima for technical assistances. This work was supported by grants from the Core Research for Evolutional Science and Technology (CREST) of Japan Science and Technology Corporation, Health and Labour Sciences Research Grants, Research on Advanced Medical Technology, nano-001, the Ministry of Agriculture, Forestry and Fisheries, and the Ministry of Health, Labor, and Welfare of Japan.

## References

[1] S.B. Prusiner, Prions, Proc. Natl. Acad. Sci. USA 95 (1998) 13363–13383.
[2] S.B. Prusiner, Shattuck lecture—neurodegenerative diseases and prions, N. Engl. J. Med. 344 (2001) 1516–1526.
[3] J. Collinge, Variant creutzfeldt-Jakob disease, Lancet 354 (1999) 317–323.
[4] N.S. Hachiya, K. Watanabe, Y. Sakasegawa, K. Kaneko, Microtubules-associated intracellular localization of the NH(2)-terminal cellular prion protein fragment, Biochem. Biophys. Res. Commun. 313 (2004) 818–823.
[5] C. Kuwahara, A.M. Takeuchi, T. Nishimura, K. Haraguchi, A. Kubosaki, Y. Matsumoto, K. Saeki, T. Yokoyama, S. Itohara, T. Onodera, Prions prevent neuronal cell-line death, Nature 400 (1999) 225–226.
[6] N.S. Hachiya, K. Watanabe, M. Yamada, Y. Sakasegawa, K. Kaneko, Anterograde and retrograde intracellular trafficking of fluorescent cellular prion protein, Biochem. Biophys. Res. Commun. 315 (2004) 802–807.
[7] K.S. Lee, A.C. Magalhaes, S.M. Zanata, R.R. Brentani, V.R. Martins, M.A. Prado, Internalization of mammalian fluorescent cellular prion protein and N-terminal deletion mutants in living cells, J. Neurochem. 79 (2001) 79–87.
[8] A.C. Magalhaes, J.A. Silva, K.S. Lee, V.R. Martins, V.F. Prado, S.S.G. Ferguson, M.V. Gomez, R.R. Brentani, M.A.M. Prado, Endocytic intermediates involved with the intracellular trafficking of a fluorescent cellular prion protein, J. Biol. Chem. 277 (2002) 33311–33318.
[9] A. Negro, C. Ballarin, A. Bertoli, M.L. Massimino, M.C. Sorgato, The metabolism and imaging in live cells of the bovine prion protein in its native form or carrying single amino acid substitutions, Mol. Cell. Neurosci. 17 (2001) 521–538.
[10] H. Lorenz, O. Windl, H.A. Kretzschmar, Cellular phenotyping of secretory and nuclear prion proteins associated with inherited prion diseases, J. Biol. Chem. 277 (2002) 8508–8516.
[11] L. Ivanova, S. Barmada, T. Kummer, D.A. Harris, Mutant prion proteins are partially retained in the endoplasmic reticulum, J. Biol. Chem. 276 (2001) 42409–42421.
[12] T. Kitamoto, R. Iizuka, J. Tateishi, An amber mutation of prion protein in Gerstmann–Straussler syndrome with mutant PrP plaques, Biochem. Biophys. Res. Commun. 192 (1993) 525–531.
[13] G. Zanusso, R.B. Petersen, T. Jin, Y. Jing, R. Kanoush, S. Ferrari, P. Gambetti, N. Singh, Proteasomal degradation and N-terminal protease resistance of the codon 145 mutant prion protein, J. Biol. Chem. 274 (1999) 23396–23404.
[14] M.R. Scott, R. Kohler, D. Foster, S.B. Prusiner, Chimeric prion protein expression in cultured cells and transgenic mice, Protein Sci. 1 (1992) 986–997.
[15] N.S. Hachiya, M. Yamada, K. Watanabe, A. Jozuka, T. Ohkubo, K. Sano, Y. Takeuchi, Y. Kozuka, Y. Sakasegawa, K. Kaneko, Mitochondrial localization of cellular prion protein (PrPC) invokes neuronal apoptosis in aged transgenic mice overexpressing PrPC, Neurosci. Lett., in press.
[16] D.A. Butler, M.A. Scott, J.M. Bockman, D.R. Borchelt, A. Taraboulos, K.K. Hsiao, D.T. Kingsbury, S.B. Prusiner, Scrapie-infected murine neuroblastoma cells produce protease-resistant prion proteins, J. Virol. 62 (1988) 1558–1564.
[17] J. Tateishi, T. Kitamoto, Inherited prion diseases and transmission to rodents, Brain Pathol. 5 (1995) 53–59.
[18] J. Ma, R. Wollmann, S. Lindquist, Neurotoxicity and neurodegeneration when PrP accumulates in the cytosol, Science 298 (2002) 1781–1785.
[19] E. Cohen, A. Taraboulos, Scrapie-like prion protein accumulates in aggresomes of cyclosporin A-treated cells, EMBO J. 22 (2003) 404–417.
[20] E. Paitel, C. Alves da Costa, D. Vilette, J. Grassi, F. Checler, Overexpression of PrPc triggers caspase 3 activation: potentiation by proteasome inhibitors and blockade by anti-PrP antibodies, J. Neurochem. 83 (2002) 1208–1214.
[21] D. Westaway, J. Cayetano-Canlas, D. Groth, D. Foster, S.-L. Yang, M. Torchia, G.A. Carlson, S.B. Prusiner, Degeneration of skeletal muscle, peripheral nerves, and the central nervous system in transgenic mice overexpressing wild-type prion proteins, Cell 76 (1994) 117–129.
[22] V. Perrier, K. Kaneko, J. Safar, J. Vergara, P. Tremblay, S.J. DeArmond, F.E. Cohen, S.B. Prusiner, A.C. Wallace, Dominant-negative inhibition of prion replication in transgenic mice, Proc. Natl. Acad. Sci. USA 99 (2002) 13079–13084.
[23] M.P. McKinley, A. Taraboulos, L. Kenaga, D. Serban, A. Stieber, S.J. DeArmond, S.B. Prusiner, N. Gonatas, Ultrastructural localization of scrapie prion proteins in cytoplasmic vesicles of infected cultured cells, Lab. Invest. 65 (1991) 622–630.
[24] K. Kaneko, D. Peretz, K.M. Pan, T.C. Blochberger, H. Wille, R. Gabizon, O.H. Griffith, F.E. Cohen, M.A. Baldwin, S.B. Prusiner, Prion protein (PrP) synthetic peptides induce cellular PrP to acquire properties of the scrapie isoform, Proc. Natl. Acad. Sci. USA 92 (1995) 11160–11164.
[25] K. Kaneko, H. Wille, I. Mehlhorn, H. Zhang, H. Ball, F.E. Cohen, M.A. Baldwin, S.B. Prusiner, Molecular properties of complexes formed between the prion protein and synthetic peptides, J. Mol. Biol. 270 (1997) 574–586.
[26] B. Kundu, N.R. Maiti, E.M. Jones, K.A. Surewicz, D.L. Vanik, W.K. Surewicz, Nucleation-dependent conformational conversion of the Y145Stop variant of human prion protein: structural clues for prion propagation, Proc. Natl. Acad. Sci. USA 100 (2003) 12069–12074.
[27] R. Chiesa, P. Piccardo, E. Quaglio, B. Drisaldi, S.L. Si-Hoe, M. Takao, B. Ghetti, D.A. Harris, Molecular distinction between pathogenic and infectious properties of the prion protein, J. Virol. 77 (2003) 7611–7622.

Available online at www.sciencedirect.com
SCIENCE DIRECT®
Biochemical and Biophysical Research Communications 329 (2005) 516–521
BBRC
www.elsevier.com/locate/ybbrc

# Influence of assembly of siRNA elements into RNA-induced silencing complex by fork-siRNA duplex carrying nucleotide mismatches at the 3′- or 5′-end of the sense-stranded siRNA element

Yusuke Ohnishi [a,b], Katsushi Tokunaga [b], Hirohiko Hohjoh [a,*]

[a] *National Institute of Neuroscience, NCNP, 4-1-1 Ogawahigashi, Kodaira, Tokyo 187-8502, Japan*
[b] *Department of Human Genetics, Graduate School of Medicine, The University of Tokyo, 7-3-1 Hongo, Bunkyo-ku, Tokyo 113-0033, Japan*

Received 27 January 2005

**Abstract**

RNA interference (RNAi) is a powerful method for suppressing the expression of a gene of interest, and can be induced by 21–25 nucleotide small interfering RNA (siRNA) duplexes homologous to the silenced gene, which function as sequence-specific RNAi mediators in RNA-induced silencing complexes (RISCs). In the previous study, it was shown that fork-siRNA duplexes, whose sense-stranded siRNA elements carried a few nucleotide mismatches at the 3′-ends against the antisense-stranded siRNA elements, could enhance RNAi activity more than conventional siRNA duplexes in cultured mammalian cells. In this study, we further characterized fork-siRNA duplexes using reporter plasmids carrying target sequences complementary to the sense- or antisense-stranded siRNA elements in the untranslated region of *Renilla* luciferase. The data presented here suggest that nucleotide mismatches at either the 3′- or 5′-end of the sense-stranded siRNA elements in fork-siRNA duplexes could influence assembly of not only the antisense-stranded siRNA elements but also the sense-stranded elements into RISCs. In addition, we further suggest the possibility that there could be a positional effect of siRNA duplex on RNAi activity.
© 2005 Elsevier Inc. All rights reserved.

*Keywords:* RNA interference; Fork-siRNA; Mismatch; RNAi mediator; RISC

RNA interference (RNAi) is the process of a sequence-specific post-transcriptional gene silencing triggered by double-stranded RNAs (dsRNAs) homologous to the silenced gene (reviewed in [1–4]). DsRNAs introduced or generated in cells are subjected to digestion with an RNase III enzyme, Dicer, into 21–25 nucleotide (nt) RNA duplexes [5–8], and the resultant RNA duplexes, referred to as small interfering RNA (siRNA) duplexes, can be associated with the RNA-induced silencing complexes (RISCs) and function as sequence-specific RNAi mediators in the complexes [5,7]. In terms of rapid and potent induction of RNAi by exogenous dsRNAs, RNAi has become a powerful reverse genetic tool for suppressing the expression of a gene of interest in various species including mammals.

In mammals, direct introduction of chemically synthesized 21–25 nt siRNA duplexes into cells is often used for induction of RNAi [9–12], although different siRNAs induce different levels of RNAi activities [10,13]. In previous studies, where the effect of various types of synthetic siRNAs on the induction of mammalian RNAi was tested, an improvement of the siRNA duplexes for enhancing RNAi activity was found [14]. The improved siRNA duplexes, named 'fork-siRNA duplexes,' possess mismatched sequences at their termini due to introduction of base substitutions into the

* Corresponding author. Fax: +81 42 346 1748.
*E-mail address:* hohjohh@ncnp.go.jp (H. Hohjoh).

0006-291X/$ - see front matter © 2005 Elsevier Inc. All rights reserved.
doi:10.1016/j.bbrc.2005.02.012

3′-ends of the sense-stranded siRNA elements: one of the ends of the fork-siRNA duplex, on the 3′-end of the sense-stranded siRNA element, remains open (unannealed). In addition to the properties of fork-siRNA duplex, recent studies suggested that siRNA duplexes conferring a strong RNAi activity could be characterized by a low base-stability due to AU-rich sequences around the 3′-ends of the sense-stranded siRNA elements, i.e., the functional siRNA duplexes have the asymmetrical features of the AU (or GC) content in their sequences [14–16]. Based on these observations, a model was proposed: the ease of unwinding from one of the ends of the siRNA duplex could determine the orientation of the duplex, and the siRNA element unwound from the 5′-end could be determined and function as a sequence-specific RNAi mediator in RISC [14].

In order to further characterize fork-siRNA duplexes, we report herein the construction of reporter plasmids carrying target sequences complementary to the sense- and antisense-stranded siRNA elements, and examination of the levels of gene silencing depending upon the sense- and antisense-stranded siRNA elements functioning as RNAi mediators in RISCs. The data presented here suggested that the structural features of fork-siRNA duplexes could influence incorporation of their siRNA elements into RISCs.

## Materials and methods

*Preparation of oligonucleotides.* RNA and DNA synthetic oligonucleotides were obtained from PROLIGO and INVITROGEN, respectively. For preparation of duplexes, sense- and antisense-stranded oligonucleotides (20 μM each) were mixed in an annealing buffer (30 μM Hepes, pH 7.4, 100 μM potassium acetate, and 2 μM magnesium acetate), heat-denatured at 90 °C for 3 min, and annealed at 37 °C overnight. The siRNA duplexes used in this study were as follows: the La21-conv. siRNA duplex (a conventional siRNA duplex), La21-3′m2 siRNA duplex (a fork-siRNA duplex carrying two-base mismatches at the 3′-end of the sense-stranded siRNA element), La21-5′m2 siRNA duplex (a fork-siRNA duplex carrying two-base mismatches at the 5′-end of the sense-stranded siRNA element), and La21-ss19 siRNA duplex (a siRNA duplex containing 19 nt sense-stranded siRNA element) (Fig. 1B) [14]. Note that these La21 siRNA duplexes possess the same antisense-stranded siRNA elements. Non-silencing siRNA duplex (Qiagen) was used as a negative control.

*Construction of reporter plasmids.* In order to insert target sequence complementary to the sense- or antisense-stranded La21 siRNA element [10] against *Photinus* luciferase in the 3′ untranslated region (UTR) of the *Renilla* luciferase transcripts, the phRL-TK plasmid (Promega) carrying the *Renilla* luciferase gene was digested with *Xba*I and *Not*I, and subjected to ligation with synthetic oligonucleotide duplexes carrying the La21 siRNA target sequences. The sequences of the synthesized oligonucleotides were as follows:

sLa21Fw; 5′-CTAGCATGCAACCGCTGGAGAGCAACTGCA-3′
asLa21Fw; 5′-GGCCTGCAGTTGCTCTCCAGCGGTTGCATG-3′
sLa21Rv; 5′-CTAGCATGCAGCAGTTGCTCTCCAGCGGTA-3′
asLa21Rv; 5′-GGCCTACCGCTGGAGAGCAACTGCTGCATG-3′

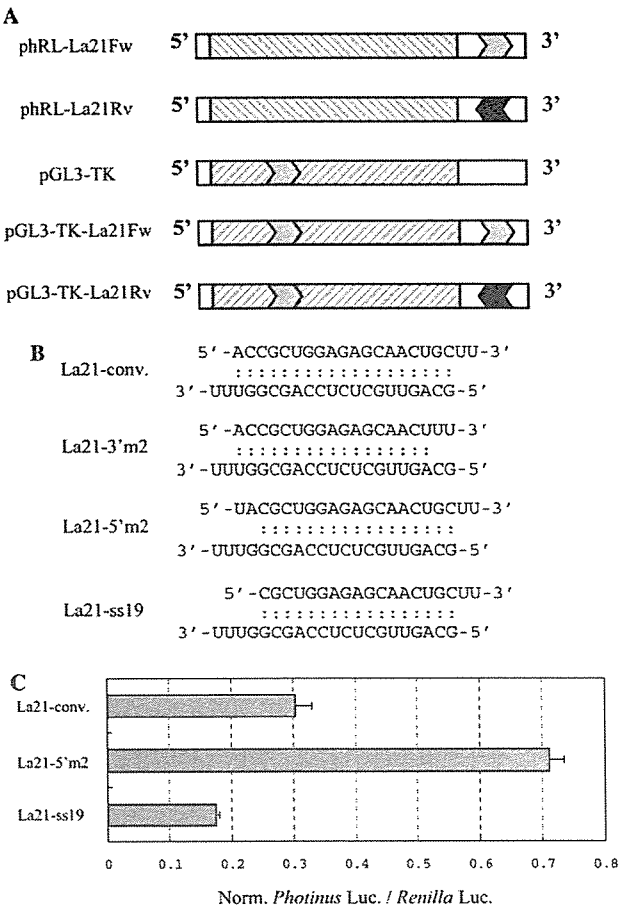


Fig. 1. Schematic drawing of the luciferase transcripts derived from plasmids constructed in this study (A), used synthetic siRNA duplexes (B), and RNAi activities induced by the siRNA duplexes (C). (A) The names of constructed plasmids are indicated. Hatched and open boxes represent the luciferase coding and untranslated regions, respectively. Gray and solid (black) regions indicate target sequences complementary to the antisense- and sense-stranded La21 siRNA elements, respectively. (B) The names of synthetic La21 siRNA duplexes are indicated. Upper and lower sequences in the duplexes represent the sense- and antisense-stranded siRNA elements, respectively. (C) Gene silencing of the *Photinus* luciferase gene. RNAi induction was carried out as described previously [14]. Indicated La21 siRNA duplexes together with pGL3-control and phRL-TK plasmids carrying *Photinus* and *Renilla* luciferase genes, respectively, were transfected into HeLa cells. Twenty-four hours after transfection, cell lysate was prepared and the level of luciferase activity was examined. Ratios of normalized target (*Photinus*) luciferase activity to control (*Renilla*) luciferase activity are shown: the ratios of luciferase activity determined in the presence of the La21 siRNA duplexes were normalized to the ratio obtained for a control in the presence of a non-silencing siRNA duplex (Qiagen). Data are averages of at least three independent determinations. Error bars represent standard deviations.

The resultant plasmids possessing the target sequences for the antisense- and sense-stranded La21 siRNA elements were named 'phRL-La21Fw' and 'phRL-La21Rv,' respectively.

We further constructed reporter plasmids carrying two target sites of the La21 siRNA duplex. The *Hin*dIII–*Xba*I fragment encoding the *Photinus* luciferase gene was isolated from the pGL3-control plasmid

(Promega), and substituted for the *Hin*dIII–*Xba*I regions carrying *Renilla* luciferase in the phRL-La21Fw and phRL-La21Rv plasmids. The resultant plasmids derived from the phRL-La21Fw and phRL-La21Rv plasmids were named 'pGL3-TK-La21Fw' and 'pGL3-TK-La21Rv,' respectively, and possessed two La21 siRNA duplex target sites, one in the *Photinus* luciferase coding region and the other in the 3′ UTR. We also constructed 'pGL3-TK' plasmid by substitution of *Photinus* luciferase for *Renilla* luciferase in the phRL-TK plasmid using the same procedure described above.

*Cell culture, transfection, and luciferase and β-galactosidase assays.* HeLa cells were grown as described previously [10]. The day before transfection, cells were trypsinized, diluted with fresh medium without antibiotics, and seeded into 24-well culture plates (approximately $0.5 \times 10^5$ cells/well). Cotransfection of synthetic siRNA duplexes with reporter plasmids was carried out using Lipofectamine 2000 transfection reagent (Invitrogen) according to the manufacturer's instructions, and to each well, 0.24 μg siRNA duplexes, 0.05 μg phRL-La21Fw or phRL-La21Rv plasmid, and 0.1 μg pSV-β-galactosidase control vector (Promega) as a control were applied. Twenty-four hours after transfection, cell lysate was prepared and the expression levels of luciferase and β-galactosidase were examined by a Dual-Luciferase reporter assay system (Promega) and a Beta-Glo assay system (Promega), respectively, according to the manufacturer's instructions. In the case of transfection with pGL3-TK, pGL3-Tk-La21Fw or pGL3-TK-La21Rv, 0.24 μg siRNA duplexes, 0.1 μg of any one of the pGL3-TK, pGL3-Tk-La21Fw, and pGL3-TK-La21Rv plasmids, and 0.05 μg of the phRL-TK plasmid as a control were applied into HeLa cells. Twenty-four hours after transfection, a Dual-Luciferase reporter assay was conducted.

## Results and discussion

### *Influence of assembly of siRNA elements into RISCs by fork-siRNA duplexes*

In the previous study, it was shown that fork-siRNA duplexes carrying nucleotide mismatches at the 3′-ends of the sense-stranded siRNA elements could enhance RNAi activity more than conventional siRNA duplexes [14]. This suggests the possibility of greater occurrence of assembly of the antisense-stranded siRNA elements rather than the sense-stranded elements into RISCs in fork-siRNA duplexes over that in conventional duplexes. Accordingly, we attempted to examine whether fork-siRNA duplexes could influence incorporation of their siRNA elements into RISCs. To address this, we constructed two reporter plasmids, phRL-La21Rv and phRL-La21Fw, carrying the target sequences for the sense- and antisense-stranded La21 siRNA elements, respectively, in the 3′ untranslated region (UTR) of *Renilla* luciferase (Fig. 1A). This is because the previous study showed that the La21-conv., La21-3′m2, and La21-5′m2 siRNA duplexes (Fig. 1B) could confer different levels of RNAi activities, although they possessed the same antisense-stranded siRNA element [14]. In addition to the previous results, the result with a newly designed siRNA duplex, the La21-ss19 siRNA duplex (Figs. 1B and C), also supported the idea that the forked terminus of siRNA duplex could influence RNAi activity. Accordingly, we decided to use the sequences of the sense- and antisense-stranded La21 siRNA elements as targets in this study. Using the phRL-La21Fw and -La21Rv plasmids, and a series of the La21 siRNA duplexes, the levels of gene silencing depending upon the sense- and antisense-stranded La21 siRNA elements were investigated.

First we examined if the sense-stranded siRNA elements, like the antisense-stranded siRNA elements, could have potential for functioning as sequence-specific RNAi mediators in RISCs. To see this, the La21-conv. siRNA duplex together with phRL-La21Rv, phRL-La21Fw or phRL-TK and pSV-β-galactosidase control vector as a control were cotransfected into HeLa cells, and the levels of the expression of *Renilla* luciferase were examined. As a result, significant suppression of the expression of *Renilla* luciferase was detectable in the presence of either phRL-La21Rv or phRL-La21Fw, whereas little or no suppression was seen in the presence of phRL-TK as a negative control (Fig. 2). Therefore, these results strongly suggest that either the sense- or antisense-stranded La21 siRNA element can be incorporated into RISC and function as a sequence-specific RNAi mediator in the complex.

We next examined the RNAi activities directed by the sense- and antisense-stranded siRNA elements derived from the La21-3′m2 and La21-5′m2 siRNA duplexes (fork-siRNA duplexes) as well as the La21-conv. siRNA duplex. As shown in Fig. 3A, when the phRL-La21Fw plasmid was used, ~86%, 95%, and 72% gene silencing mediated by the antisense-stranded La21 siRNA elements derived from the La21-conv., La21-3′m2, and

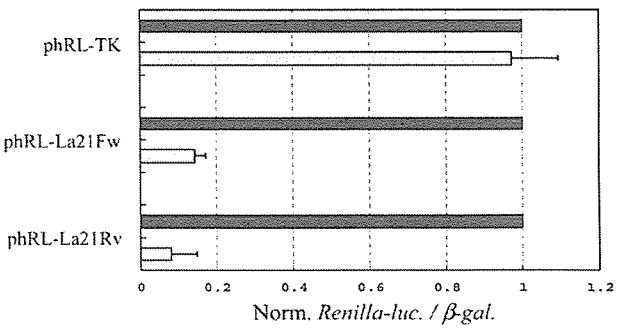


Fig. 2. Gene silencing of exogenous reporter gene with conventional siRNA duplexes. The conventional La21 (La21-conv.) siRNA duplex against the *Photinus* luciferase gene together with phRL-TK, phRL-La21Fw, or phRL-La21Rv plasmid carrying the *Renilla* luciferase reporter gene, and pSV-β-galactosidase control vector as a control were cotransfected into HeLa cells. Twenty-four hours after transfection, cell lysate was prepared, and the levels of the luciferase and β-galactosidase activities were examined. Ratios of normalized target (*Renilla*) luciferase activity to control β-galactosidase activity are shown: the ratios of luciferase activity determined in the presence of the La21-conv. siRNA duplex (gray bars) are normalized to the ratio obtained for a control in the presence of a non-silencing siRNA duplex (Qiagen) (solid bars). Data are averages of at least four independent experiments. Error bars represent standard deviations.

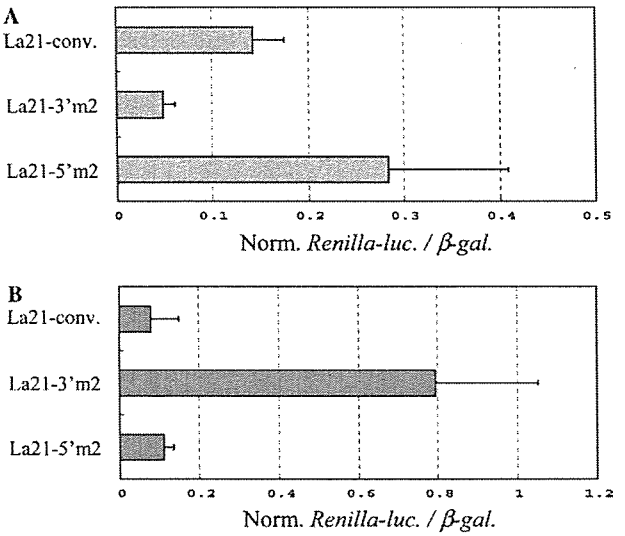


Fig. 3. Silencing of the expression of exogenous reporter gene with various types of siRNA duplexes. The conventional La21 (La21-conv.) or fork-La21 (La21-3′m2 and La21-5′m2) siRNA duplexes together with phRL-La21Fw (A) or phRL-La21Rv (B) reporter plasmid and pSV-β-galactosidase control vector as a control were cotransfected into HeLa cells, and the expression levels of luciferase and β-galactosidase were examined as in Fig. 2. Ratios of normalized target (*Renilla*) luciferase activity to control β-galactosidase activity are shown as in Fig. 2. Data are averages of at least four independent determinations. Error bars indicate standard deviations.

La21-5′m2 siRNA duplexes, respectively, was observed. Although the levels of the gene silencing with phRL-La21Fw as a reporter plasmid increased further than those with the pGL3-control plasmid carrying *Photinus* luciferase in the previous study [14] (further discussion below), the effects of mismatches at the 3′- and 5′-ends of the sense-stranded elements in the La21 fork-siRNA duplexes on RNAi activity appeared to remain unchanged in the experiments using either phRL-La21Fw or pGL3-control.

When the phRL-La21Rv plasmid was used, i.e., when the levels of the RNAi activity directed by the sense-stranded La21 siRNA elements were examined, significant differences in the level of RNAi activity among the La21 siRNA duplexes used were observed: while ~92% and 89% suppression of the expression of *Renilla* luciferase was detectable in the presence of the La21-conv., and La21-5′m2 siRNA duplexes, respectively, the gene silencing mediated by the sense-stranded element derived from the La21-3′m2 duplex appeared to confer ~20% inhibition of the expression of *Renilla* luciferase (Fig. 3B), suggesting that the degree of assembly of the sense-stranded siRNA element into RISC in the La21-3′m2 siRNA duplex could be much lower than those in the La21-conv., and La21-5′m2 siRNA duplexes. Taking all the data together, these observations suggest that nucleotide mismatches at the ends of fork-siRNA duplexes can influence assembly of not only the antisense-stranded siRNA elements but also the sense-stranded siRNA elements into RISCs.

The previous in vitro RNAi reaction with *Drosophila* embryo lysate has demonstrated that single nucleotide mismatch around the termini of siRNA duplex can affect target-RNA cleavages directed by the sense- and antisense-stranded siRNA elements [15]. The results of our present study using cultured human cells consistently agree with those in the previous study. Therefore, it appears that the effect of low base-pairing stabilities due to either AU-rich or nucleotide mismatches around the termini of siRNA duplexes on RNAi activity is likely common among various species. In addition, such low base-pairing stability could contribute to ready unwinding of the duplex from that end by a possible helicase activity in RISCs.

Another important point to note in this study is that the sense-stranded siRNA elements have potential for functioning as sequence-specific RNAi mediators in RISCs. As previously suggested [14], this indicates that off-target gene silencing mediated by the sense-stranded siRNA elements could occur in RNAi induction by siRNA duplexes. Our present data also indicated a possible avoidance of such off-target gene silencing: fork-siRNA duplexes carrying nucleotide mismatches at the 3′-end of the sense-stranded elements could reduce such off-target silencing. Therefore, fork-siRNA duplexes may provide us with not only an increase in RNAi activity but also decrease in off-target gene silencing directed by the sense-stranded siRNA elements.

### *Positional effect of siRNA target site on RNAi activity*

The results shown in Fig. 3A led us to the possibility that the position of an siRNA target site on a silenced gene transcript could influence its RNAi activity, i.e., there could be a positional effect of the siRNA target site on RNAi activity. To examine this possibility, we constructed two reporter plasmids carrying *Photinus* luciferase, pGL3-TK-La21Rv and pGL3-TK-La21Fw, whose 3′ UTRs contained the target sequences complementary to the sense- and antisense-stranded La21 siRNA elements, respectively (Fig. 1A). Thus, the resultant *Photinus* luciferase transcripts derived from pGL3-TK-La21Fw and pGL3-TK-La21Rv possess two target sites: one site complementary to the antisense-stranded La21 siRNA element is in the luciferase coding region, and the other complementary to the sense- or antisense-stranded siRNA element is in its 3′ UTR.

The La21-conv., La21-3′m2, or La21-5′m2 siRNA duplexes together with the pGL3-TK (carrying one target site in the luciferase coding region), pGL3-TK-La21Rv or pGL3-TK-La21Fw plasmid (Fig. 1A) and the phRL-TK plasmid as a control were cotransfected into HeLa cells, and the levels of RNAi activity were examined by a dual-luciferase assay. When the

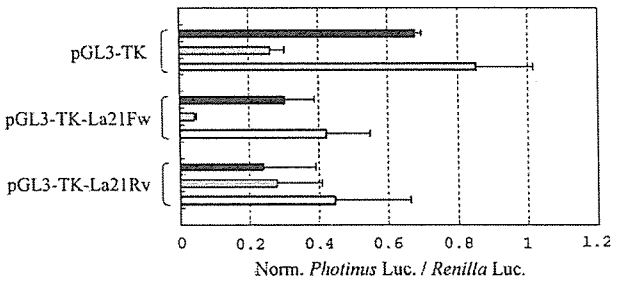


Fig. 4. Gene silencing of *Photinus* luciferase carrying two target sites of the La21 siRNA duplex. The La21-conv., La21-3′m2 or La21-5′m2 siRNA duplex together with pGL3-TK, pGL3-TK-La21Fw or pGL3-TK-La21Rv reporter plasmid carrying *Photinus* luciferase and phRL-TK plasmid carrying *Renilla* luciferase as a control were cotransfected into HeLa cells, and the expression levels of luciferase were examined as in Fig. 1. Ratios of normalized target (*Photinus*) luciferase activity to control (*Renilla*) luciferase activity are shown as in Fig. 1. Solid, gray, and open bars indicate the data in the presence of the La21-conv., La21-3′m2, and La215′m2 siRNA duplexes, respectively. Data are averages of at least three independent determinations. Error bars represent standard deviations.

pGL3-TK plasmid was used, results similar to those in the previous study using the pGL3-control plasmid encoding *Photinus* luciferase driven by the SV40 promoter [14] were observed (Fig. 4). When the pGL3-TK-La21Fw and pGL3-TK-La21Rv plasmids were used, the levels of RNAi activity, other than those in the presence of the pGL3-TK-La21Rv plasmid and the La21-3′m2 siRNA duplex, appeared to increase more greatly in both the pGL3-TK-La21Fw and pGL3-TK-La21Rv plasmids than in the pGL3-TK plasmid used, suggesting that two target sites of the La21 siRNA duplex on the silenced *Photinus* luciferase transcript probably contributed to the enhancement of RNAi activity. As for the RNAi activity in the presence of pGL3-TK-La21Rv and the La21-3′m2 siRNA duplex, it may be that the target site in the luciferase coding region, not in the 3′ UTR, is only recognizable for active RISCs, since a rather weak RNAi activity mediated by the sense-stranded siRNA element in the La21-3′m2 siRNA duplex was detected in the presence of phRL-La21Rv (Fig. 3B). This may account for the lack of significant difference in the level of RNAi activity between pGL3-TK and pGL3-TK-La21Rv in the presence of the La21-3′m2 siRNA duplex.

It should be noted that the La21-5′m2 siRNA duplex was able to confer ~60% suppression of the expression of *Photinus* luciferase in pGL3-TK-La21Fw, although the duplex was able to induce ~15% inhibition of the *Photinus* luciferase expression in pGL3-TK. Since the *Photinus* luciferase transcripts derived from pGL3-TK-La21Fw carry two identical target sites complementary to the antisense-stranded La21 siRNA element, and since the target site in the luciferase coding region appeared not to contribute much to gene silencing when using the La21-5′m2 siRNA duplex (Fig. 4), it is conceivable that the target site in the 3′ UTR could be more sensitive to cleavage by RISCs than that in the luciferase coding region on the *Photinus* luciferase transcripts derived from pGL3-TK-La21Fw in the presence of the La21-5′m2 siRNA duplex. These observations thus suggest a possible positional effect of target site of siRNA duplex on RNAi activity.

Finally, we add that a difference in RNAi activity between phRL-La21Rv (Fig. 3) and pGL3-TK-La21Rv in the presence of the La21-5′m2 siRNA duplex was observed, although the *Renilla* and *Photinus* luciferase transcripts derived from phRL-La21Rv and pGL3-TK-La21Rv, respectively, which carried the same target sites complementary to the sense-stranded La21 siRNA element in their 3′ UTRs, could be subjected to gene silencing chiefly mediated by the sense-stranded siRNA element. The difference might be attributable to possibly different stabilities between the *Renilla* and *Photinus* luciferase gene products in cells. To further evaluate such a possible difference and also the positional effect of siRNA target site on RNAi activity, more extensive studies need to be carried out.

## Acknowledgments

We thank Dr. K. Kaneko for his encouragement and support. We also thank Y. Tamura and K. Omi for their helpful cooperation. This work was supported in part by research grants from the Ministry of Health, Labor, Welfare in Japan, and by a Grant-in-Aid from the Japan Society for the Promotion of Science.

## References

[1] P.A. Sharp, RNAi and double-strand RNA, Genes Dev. 13 (1999) 139–141.
[2] J.M. Bosher, M. Labouesse, RNA interference: genetic wand and genetic watchdog, Nat. Cell. Biol. 2 (2000) E31–E36.
[3] H. Vaucheret, C. Beclin, M. Fagard, Post-transcriptional gene silencing in plants, J. Cell Sci. 114 (2001) 3083–3091.
[4] H. Cerutti, RNA interference: traveling in the cell and gaining functions? Trends Genet. 19 (2003) 39–46.
[5] S.M. Hammond, E. Bernstein, D. Beach, G.J. Hannon, An RNA-directed nuclease mediates post-transcriptional gene silencing in *Drosophila* cells, Nature 404 (2000) 293–296.
[6] P.D. Zamore, T. Tuschl, P.A. Sharp, D.P. Bartel, RNAi: double-stranded RNA directs the ATP-dependent cleavage of mRNA at 21 to 23 nucleotide intervals, Cell 101 (2000) 25–33.
[7] E. Bernstein, A.A. Caudy, S.M. Hammond, G.J. Hannon, Role for a bidentate ribonuclease in the initiation step of RNA interference, Nature 409 (2001) 363–366.
[8] S.M. Elbashir, W. Lendeckel, T. Tuschl, RNA interference is mediated by 21- and 22-nucleotide RNAs, Genes Dev. 15 (2001) 188–200.
[9] S.M. Elbashir, J. Harborth, W. Lendeckel, A. Yalcin, K. Weber, T. Tuschl, Duplexes of 21-nucleotide RNAs mediate RNA

interference in cultured mammalian cells, Nature 411 (2001) 494–498.
[10] H. Hohjoh, RNA interference (RNAi) induction with various types of synthetic oligonucleotide duplexes in cultured human cells, FEBS Lett. 521 (2002) 195–199.
[11] K. Omi, K. Tokunaga, H. Hohjoh, Long-lasting RNAi activity in mammalian neurons, FEBS Lett. 558 (2004) 89–95.
[12] N. Sago, K. Omi, Y. Tamura, H. Kunugi, T. Toyo-oka, K. Tokunaga, H. Hohjoh, RNAi induction and activation in mammalian muscle cells where Dicer and eIF2C translation initiation factors are barely expressed, Biochem. Biophys. Res. Commun. 319 (2004) 50–57.
[13] T. Holen, M. Amarzguioui, M.T. Wiiger, E. Babaie, H. Prydz, Positional effects of short interfering RNAs targeting the human coagulation trigger tissue factor, Nucleic Acids Res. 30 (2002) 1757–1766.
[14] H. Hohjoh, Enhancement of RNAi activity by improved siRNA duplexes, FEBS Lett. 557 (2004) 193–198.
[15] D.S. Schwarz, G. Hutvagner, T. Du, Z. Xu, N. Aronin, P.D. Zamore, Asymmetry in the assembly of the RNAi enzyme complex, Cell 115 (2003) 199–208.
[16] A. Khvorova, A. Reynolds, S.D. Jayasena, Functional siRNAs and miRNAs exhibit strand bias, Cell 115 (2003) 209–216.

*Amyloid*, March 2006; 13(1): 1–5

Taylor & Francis
Taylor & Francis Group

# Three-repeat Tau 69 is a major tau isoform in laser-microdissected Pick bodies

TAKUYA OHKUBO[1,2], YUJI SAKASEGAWA[3], HIROYUKI TODA[4], HITARU KISHIDA[4], KUNIMASA ARIMA[5], MITSUNORI YAMADA[6], HITOSHI TAKAHASHI[6], HIDEHIRO MIZUSAWA[2], NAOMI S. HACHIYA[1], & KIYOTOSHI KANEKO[1]

[1]*Second Department of Physiology, Tokyo Medical University, Tokyo, Japan,* [2]*Department of Neurology and Neurological Science, Graduate School of Medicine, Tokyo Medical and Dental University, Tokyo, Japan,* [3]*Department of Prion Protein Research, Tohoku University, Sendai, Japan,* [4]*Department of Neurology, Yokohama City University School of Medicine, Yokohama, Japan,* [5]*Department of Laboratory Medicine, National Center Hospital for Mental Nervous and Muscular Disorders, National Center of Neurology and Psychiatry, Tokyo, Japan, and* [6]*Department of Pathology, Brain Research Institute, Niigata University, Niigata, Japan*

**Keywords:** *Pick's disease, Pick body, Laser Microdissection System, phosphorylated tau, Tau 60, Tau 64, Tau 69*

**Abbreviations:** *LMDS-WB = Laser Microdissection System and Western blot analysis; PB = Pick body*

**Abstract**

By utilizing a novel combinatorial method of a Laser Microdissection System and Western blot analysis, we demonstrate that a distinct isoform of abnormally phosphorylated tau (69 kDa, Tau 69) predominantly aggregated in laser-microdissected Pick bodies (PBs) in sporadic Pick's disease. By contrast, tau migrated as two major bands of 60 and 64 kDa (Tau 60 and 64) in total brain homogenates as previously reported. Comparative immunohistochemical analysis with anti–4-repeat antibody revealed that a major component of the abnormally phosphorylated tau in these PBs was 3-repeat tau (3R-tau). Whether 29 amino acid repeat encoded by exons 2 and 3 in the Tau 69 might accelerate the formation of PBs remains to be further investigated. Such a combination of morphological and biochemical techniques significantly complements the existing histopathological methods.

## Introduction

Pick's disease is a type of progressive presenile dementia, characterized by a frontotemporal cortical atrophy, widespread white matter degeneration and intraneuronal lesions denoted as Pick bodies (PBs), of which the major structural components are tau proteins. Abnormally phorphorylated tau proteins have been investigated by classical biochemical methods, and tau doublet (Tau 60 and Tau 64) was detected from brain homogenates in these patients [1–3] but not detected from normal brain homogenates, because tau proteins are not abnormally phosphorylated in normal brain [4].

Here we established a novel combinatorial method of a Laser Microdissection System [5] and Western blot analysis (LMDS-WB) which enables us to examine the molecular profile of proteins in microscopic regions of interest. Hence, we applied this novel method to examine PBs in Pick's disease, a sporadic tauopathy of progressive presenile dementia [6]. Subsequently, we identified a distinct pattern of tau isoforms in the laser-microdissected PBs, which was clearly different from those detected in total brain homogenates. These data suggest that a novel tau region is associated with the formation of PBs, other than the microtubule-binding motifs, in sporadic Pick's disease.

## Materials and methods

### *Patients*

Temporal cortexes from 2 patients with sporadic Pick's disease (patient 1 [sPiD1]; female, 55 years and patient 2 [sPiD2]; female, 76 years) were obtained from the National Center of Neurology and Psychiatry, Brain Research Institute, Niigata University. The sPiD1 was previously reported as

Correspondence: Dr Kiyotoshi Kaneko, Second Department of Physiology, Tokyo Medical University, 6-1-1 Shinjuku, Shinjuku-ku, Tokyo 160-8402, Japan. Tel: 81 3 3351 6141. ext. 322. Fax: 81 3 3351 6544. E-mail: k-kaneko@tokyo-med.ac.jp
The first two authors have equal contribution in this work and both are equally considered as "first author".

ISSN 1350-6129 print/ISSN 1744-2818 online © 2006 Taylor & Francis
DOI: 10.1080/13506120500535586

case 5 [7], and sPiD2 was also reported as case 2 [8]. The tissue was placed directly in a deep freezer at −80°C (sPiD1), or immediately quick-frozen in cold isopentane and kept in a deep freezer at −80°C (sPiD2) until use.

*Laser-microdissection and Western blot analysis*

The slide preparations for microbiochemical analysis were made by NexES® Automated Immunohistochemistry Staining System (Ventana Medical Systems, Inc., Tucson, AZ, USA). Immunostained solid samples of smaller than 10 $\mu m^3$ (Figure 1A) were dissected by our new Laser Microdissection System (Olympus Optical Co., ltd., Tokyo, Japan) coupled to HOYA laser cutter, HCL2100 (30 mJ/pulse, 266 nm, Hoya Co., Tokyo, Japan). Dissected samples were collected by the CellTram Oil®, hydraulic manual microinjector (Eppendorf, Hamburg, Germany) with distilled water. About 500 PBs were collected and analyzed each time (Figure 1B). Total brain homogenates (10 $\mu g$), laser-dissected PBs (500 pieces), and their surrounding brain tissues without PBs were solubilized in 500 $\mu l$ of ice-cold

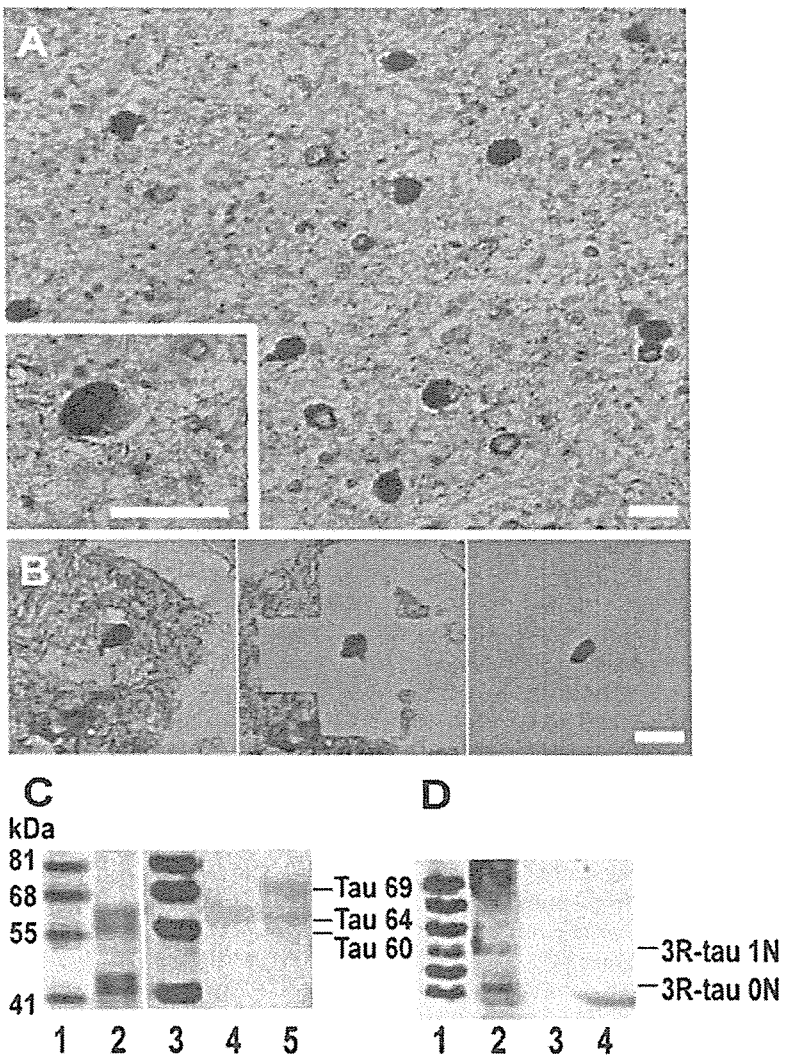


Figure 1. Temporal cortex, patient 1 with sporadic Pick's disease (sPiD1). (A) Ten-$\mu m$-thick cryosection. Pick bodies (PBs) of sPiD1 stained with AT8 (purple) and hematoxylin (blue). Scale bar is 20 $\mu m$. (B) Two-$\mu m$-thick cryosection of sPiD1. PBs isolated from the section by the Laser Microdissection System. Scale bar is 20 $\mu m$. (C) Western blot analysis of sPiD1 with AT8 and AT100 antibodies. Molecular weight marker (Dr. Western, Oriental Yeast, Tokyo, Japan, lanes 1 and 3), temporal brain homogenates (40 $\mu g$, lane 2), surrounding area of PBs (1–3 ng, lane 4), laser microdissected PBs (1–3 ng, lane 5). (D) Western blot analysis of sarkosyl-insoluble fraction of temporal brain homogenates of sPiD1 after dephosphorylation by bacterial alkaline phosphatase (8 $\mu g$, lane 2), blank lane (lane 3), and bacterial alkaline phosphatase alone (lane 4) with HT7 antibody. Molecular weight marker (six recombinant tau isoforms in lane 1; 67, 62, 59, 54, 52, and 48 kDa, respectively).

extraction buffer (Tris-chrolide (pH 7.4), 0.8 M NaCl, 1 mM EGTA, 10% sucrose and 1/1,000 w/v protease inhibitor cocktail (Sigma) with 1% sodium *N*-lauroyl sarcosinate. Sarkosyl-insoluble fractions were collected by 182,000 × *g* for 30 min at 4°C, and suspended in 50 mM Tris-chrolide (pH 7.4). The sarkosyl-insoluble material was boiled with Lammeli's buffer for 10 min at 95°C, loaded onto 12% SDS-PAGE gels and transferred onto nitrocellulose membranes. Nitrocellulose membranes were blocked with 5% non-fat milk in PBS-T and incubated with 1:1,000 AT100 (Innogenetics, Ghent, Belgium) specific to phosphorylated Thr 212/Ser 214, and 1:1,000 AT8 (Innogenetics, Ghent, Belgium) specific to phosphorylated Ser 202/Thr 205 of tau in PBS-T. Immunodecorated bands were visualized by SuperSignal West Femto Maximum Sensitivity Substrate (Pierce, Rockford, IL, USA), and analyzed using the Fluor-S MAX MultiImager or VersaDoc (Bio-Rad Laboratories, Hercules, CA, USA).

*Sarkosyl-insoluble fraction of brain samples and their dephosphorylation*

Frozen total brain sample (0.2 g) was homogenated with 500 μl of ice-cold extraction buffer (50 mM Tris-chrolide [pH 7.4], 0.8 M NaCl, 1 mM EGTA, 10% sucrose and 1/1,000 w/v protease inhibitor cocktail (Sigma)) and 1/10 volume of glassbeads. After 20,000 × *g* centrifugation for 10 min at 4°C, the supernatant was incubated with 1% sodium *N*-lauroyl sarcosinate. Sarkosyl-insoluble fractions were collected by 182,000 × *g* for 30 min at 4°C, and half of the sarkosyl-insoluble material was suspended in 50 mM Tris-chrolide (pH 7.4) for Western blot analysis of total brain sample [9].

The other half of the sarkosyl-insoluble material was used for the following dephosphorylation study. The sample was treated with 4 M guanidine hydrochloride for 1 h at room temperature, followed by overnight dialysis at 4°C against 50 mM Tris-chrolide (pH 8.8), 0.1 mM EDTA and 0.1 mM phenylmethylsulfonyl fluoride (PMSF). The sample was then incubated for 4 h at 67°C with 5 U/ml *E. coli* alkaline phosphatase (type III-N; Sigma). The incubated sample was purified with 1.5 M ammonium sulfate soloution to remove alkaline phosphatase for 1 h at room temperature. After 20,000 × *g* centrifugation for 10 min at 4°C, the pellet was suspended in 50 mM Tris-chrolide (pH 8.8) and boiled for 10 min at 95°C. The sample was then loaded onto 7.5% SDS-PAGE gels and transferred onto nitrocellulose membranes. Nitrocellulose membranes were blocked with 5% non-fat milk in phosphate buffered saline containing 0.05% Tween-20 (PBS-T) and incubated with 1:10,000 HT7 (Innogenetics, Ghent, Belgium) specific to amino acid residues 159–163 of tau in PBS-T. Immunodecorated bands were incubated with 1:10,000 horseradish peroxidase-cojugated anti-mouse IgG antibody in PBS-T, visualized by ECL plus, and analyzed using the VersaDoc.

*Construction, expression, and purification of 6 recombinant tau isoforms*

The classical Goedert's method [9] was modified as follows. Human full-length cDNA clones encoding six human tau protein isoforms were subcloned into the *Eco*RI site and *Xho*I site of pBluescript II SK+. Following cleavage with *Eco*RI and *Xho*I, the resulting cDNA fragments were subcloned downstream of the T7 RNA polymerase promoter into *Eco*RI and *Xho*I cut expression plasmid pET11a and the recombinant plasmids were transformed into *E. coli* BL21 (DE3) cells. The *E. coli* cells were grown to an optical density of 0.6–1.0 at 600 nm. Expression was induced by adding IPTG to a final concentration of 0.4 mM. After shaking for 3 h at 30°C, the cells were collected by centrifugation. The *E. coli* pellets were suspended in 50 mM PIPES (pH 6.8), 1 mM DTT, 1 mM EDTA and protease inhibitors cocktail (Sigma) and sonicated 1 × 10 min on ice using Branson Sonifier 250. The homogenates were centrifuged at 182,000 × *g* for 30 min at 4°C and the resultant supernatant was loaded onto a phosphocellulose packed column equibrated in extraction buffer.

After exhaustively washing in the same buffer, protein was eluted batchwise with 3 ml aliquots of extraction buffer containing 0.5 M NaCl. Fractions 2 and 3, which contained the recombinant tau proteins, were pooled and precipitated with 1.5 M ammonium sulfate. The pellet was washed in 50 mM PIPES (pH 6.8), 1 mM DTT, 1 mM EDTA and protease inhibitors cocktail (Sigma), and dialyzed overnight against 50 mM MES and 1 mM DTT (pH 6.5). After centrifugation the dialysate was loaded onto a Mono S HR 5/5 column (Amersham Biosciences). The column was washed with 50 mM MES, 1 mM DTT and 50 mM NaCl (pH 6.5), then the protein was eluted using a 100–300 mM NaCl gradient in 50 mM MES and 1 mM DTT (pH 6.5). Column fractions were screened by gel electrophoresis and Quick-CBB (Coomassie Brilliant Blue) PLUS stain (Wako), the peak tau fractions were pooled. Those fractions were then loaded onto a Superdex 200 HR 10/30 column (Amersham Biosciences). The column was washed with 50 mM MES, 1 mM DTT and 150 mM NaCl (pH 6.5). After screening column fractions by the same methods as above, the peak tau fractions were pooled, freezed by liquid nitrogen and stored in deep-freezer until use. After six tau isoforms

were collectively purified and measured their concentration with densitometry against bovine serum albumin, an equal volume of each of the six tau isoforms were mixed together. Five $\mu$l of this mixture were run alongside dephosphorylated sample for the molecular weight marker (Figure 1D).

*Immunohistochemistry*

Cryostat sections (2–20 $\mu$m thick) were made from the frozen material, fixed with cold acetone (−20°C) for 7 min, and immunostained by the avidin-biotin-peroxidase complex (ABC) method with a VECTASTATIN ABC elite kit (Vector Laboratories, Burlingame, CA, USA), using a mouse monoclonal antibody against phosphorylation-dependent tau proteins (AT8; Innogenetics, Ghent, Belgium, 1:200) or a rabbit antiserum against 4-repeat tau (4R-tau) (EX10; 1:2,000, kindly provided by Dr. T. Arai) [2]. For the later immunostaining, tissue sections were pretreated with 99% formic acid for 5 s. Diaminobenzidine was used as the chromogen. After immunostaining, the sections were counterstained with hematoxylin. For negative controls, the first antibodies were omitted or replaced with normal serum.

## Results

In total brain homogenates of sPiD1, tau migrated as two major bands of 60 and 64 kDa (Tau 60 and 64) by common microgram scale Western blot (Figure 1C, lane 2) as previously described [1,2]. After dephosphorylation by bacterial alkaline phosphatase (type III-N; Sigma), tau in sarkosyl-insoluble fractions appeared as two major bands that align with either 3-repeat tau (3R-tau) 0N; 3R-tau with no N-terminal amino acids inserts (dephosphorylated Tau 60), or 3R-tau 1N; 3R-tau with 29 amino acids inserts encoded by exon 2 (dephosphorylated Tau 64) [Figure 1D, lane 2].

On the other hand, tau migrated as a major band of 69 kDa (Tau 69) in laser microdissected PBs (Figure 1C, lane 5), and Tau 64 predominated in surrounding area of PBs (Figure 1C, lane 4). In order to clarify whether the Tau 69 in PBs was composed of either 3R-tau or 4R-tau, comparative immunohistochemical analysis with anti 4R-tau antibody (EX10) was performed, since EX10 was not sensitive enough for our nanogram scale Western blot analysis due to the lack of efficient immunoreactions (data not shown). Further, the amount of laser microdissected PBs was insufficient for the dephosphorylation procedure. Definite immunoreactivity for 4R-tau was barely detectable in a small population of PBs (less than 1% of the total PBs, Figure 2B), while AT8 (phosphorylation dependent anti-tau antibody)-immunohistochemistry revealed the presence of many immunoreactive PBs (Figure 2A). From these data, we concluded that a major component of PBs in these patients are 3R-tau with 58 amino acids inserts encoded by exons 2 and 3 (represented as Tau 69).

## Discussion

One possible scenario drawn from our results is that the 29 amino acid repeat in exons 2 and 3 may have a higher tendency to form PBs in a repeat-number-dependent manner, which is independent from the well-known microtubules-binding regions where tau mutations tend to cluster [10]. In fact, King et al. [11] experimentally observed that polymerization of the intact tau molecule was facilitated by the amino acid sequences in exons 2 and 3. It was also seen that insoluble tau of 69 kDa (Tau 69) predominantly

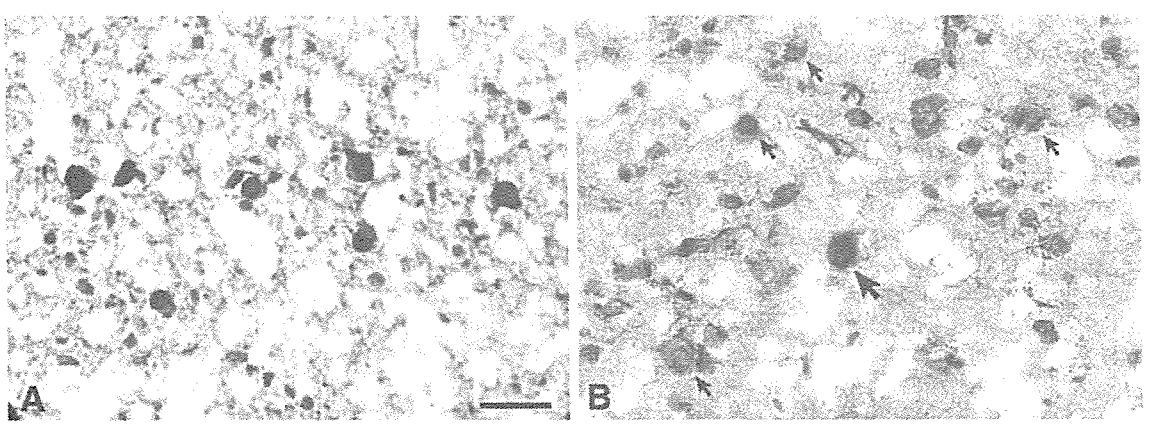


Figure 2. Immunoreactivity for phosphorylated tau (A) and 4R-tau (B) tau proteins in the second cortical layer of sPiD2. Intense labeling is present in many PBs in the panel A with AT8 antibody, but is restricted only in one PB in the panel B with EX10 antibody (large arrow). Small arrows in the panel B indicate PBs with little or no immunostaining. Scale bar is 30 $\mu$m.

accumulated in neuronal cells when normal human tau was expressed in *Caenorhabditis elegans* to model tauopathy disorders [12], which may further support our notion. Tau 69 is also observed in aggregates of other tauopathies including progressive supranuclear palsy (4R-tau) [2] and corticobasal degeneration (4R-tau) [2], or in Alzheimer's disease (3R and 4R-tau) [1]. Thus, such 29 amino acid repeats in exons 2 and 3 may also account for the formation of aggregates in these disorders.

As shown, both methods of immunohistochemistry and Western blot are mutually complementary at the microscopic level. Of note, our novel combination method (LMDS-WB) targets proteins in the specific regions of interest at the micrometer order, which was separated by SDS-PAGE and immunoblotted, and thus, exclusively enables us to gather information on the molecular profile (i.e. molecular weight) of target proteins under the microscope *in situ*. In fact, we successfully detected distinct isoforms of abnormally phosphorylated tau in PBs for the first time, something never observed from total brain homogenates with conventional approaches. However, immunohistochemistry usually exhibits a greater sensitivity compared to antibodies used for these purposes. For example, immunohistochemistry using AT8 was able to stain PBs at a single cell level, although at least a few hundred PBs were required for our combinatorial method of LMDS-WB with AT100.

Nonetheless, our method has indispensable advantages over the immunohistochemistry as shown in this study. Such a combination of morphological and biochemical techniques significantly complements the existing histopathologic methods, and has a great potential for investigating normal or abnormal microstructures in various conditions and disorders.

## Acknowledgements

We thank K. Watanabe and K. Takayama for technical assistance. This work was supported by grants from the Ministry of Health, Labor and Welfare and the Ministry of Education, Culture, Sports, Science and Technology, Japan, and the Core Research for Evolutional Science and Technology (CREST) of Japan Science and Technology Agency.

## References

1. Delacourte A, Sergeant N, Wattez A, Gauvreau D, Robitaille Y. Vulnerable neuronal subsets in Alzheimer's and Pick's disease are distinguished by their tau isoform distribution and phosphorylation. Ann Neurol 1998;43:193–204.
2. Arai T, Ikeda K, Akiyama H, Shikamoto Y, Tsuchiya K, Yagishita S, Beach T, Rogers J, Schwab C, McGeer PL. Distinct isoforms of tau aggregated in neurons and glial cells in brains of patients with Pick's disease, corticobasal degeneration and progressive supranuclear palsy. Acta Neuropathol (Berl) 2001;101:167–173.
3. Zhukareva V, Mann D, Pickering-Brown S, Uryu K, Shuck T, Shah K, Grossman M, Miller BL, Hulette CM, Feinstein SC, et al. Sporadic Pick's disease: a tauopathy characterized by a spectrum of pathological tau isoforms in gray and white matter. Ann Neurol 2002;51:730–739.
4. Sergeant N, Delacourte A, Buee L. Tau protein as a differential biomarker of tauopathies. Biochim Biophys Acta 2005;1739:179–197.
5. Tanaka T, Ito T, Furuta M, Eguchi C, Toda H, Wakabayashi-Takai E, Kaneko K. In Situ Phage Screening. A method for identification of subnanogram tissue components in situ. J Biol Chem 2002;277:30382–30387.
6. Buee L, Bussiere T, Buee-Scherrer V, Delacourte A, Hof PR. Tau protein isoforms, phosphorylation and role in neurodegenerative disorders. Brain Res Brain Res Rev 2000;33: 95–130.
7. Arima K. Involvement of subcortical nuclei and brain stem in Pick's disease: a topographical study of Pick bodies. Neuropathology 1989;9:105–115.
8. Mori F, Hayashi S, Yamagishi S, Yoshimoto M, Yagihashi S, Takahashi H, Wakabayashi K. Pick's disease: alpha- and beta-synuclein-immunoreactive Pick bodies in the dentate gyrus. Acta Neuropathol (Berl) 2002;104:455–461.
9. Goedert M, Spillantini MG, Cairns NJ, Crowther RA. Tau proteins of Alzheimer paired helical filaments: abnormal phosphorylation of all six brain isoforms. Neuron 1992;8: 159–168.
10. Lee VM, Goedert M, Trojanowski JQ. Neurodegenerative tauopathies. Annu Rev Neurosci 2001;24:1121–1159.
11. King ME, Gamblin TC, Kuret J, Binder LI. Differential assembly of human tau isoforms in the presence of arachidonic acid. J Neurochem 2000;74:1749–1757.
12. Kraemer BC, Zhang B, Leverenz JB, Thomas JH, Trojanowski JQ, Schellenberg GD. Neurodegeneration and defective neurotransmission in a Caenorhabditis elegans model of tauopathy. Proc Natl Acad Sci USA 2003;100: 9980–9985.

Medical Hypotheses (2007) 68, 670–673

ELSEVIER

medical hypotheses

http://intl.elsevierhealth.com/journals/mehy

# The possible role of protein X, a putative auxiliary factor in pathological prion replication, in regulating a physiological endoproteolytic cleavage of cellular prion protein

Naomi S. Hachiya, Midori Imagawa, Kiyotoshi Kaneko *

*Department of Neurophysiology, Tokyo Medical University, 6-1-1 Shinjuku, Tokyo 160-8402, Japan*

Received 9 July 2006; accepted 19 July 2006

**Summary** The posttranslational conformational conversion of the cellular isoform of prion protein $PrP^{C}$ into its scrapie isoform $PrP^{Sc}$ is the fundamental process underlying the pathogenesis of prion disease. Based on several transgenic data, it has been postulated that a putative auxiliary factor denoted protein X functions as a molecular chaperone through its unfolding activity of $PrP^{C}$ during the formation of $PrP^{Sc}$. However, the assumption that protein X therefore exists exclusively in prion diseases appears improbable and thus, it should have some simultaneous physiological role. We, hereby, propose a novel concept – a characteristic role of protein X in supporting a physiological endoproteolytic cleavage of $PrP^{C}$. The events corresponding to the formation of the physiologically metabolized $PrP^{C}$ or the pathologically transformed $PrP^{Sc}$ are mutually exclusive. Amino acid residues that are critical in terms of the target site of protein X for the pathological alteration into $PrP^{Sc}$ overlap at the cleavage site. These amino acid residues tend to have a hydrophobic property and are most probably found buried inside the native protein structure. Therefore, a putative molecular chaperone identical to protein X may target the same hydrophobic residues in $PrP^{C}$ and work in conjunction with either $PrP^{Sc}$ in prion disease or PrP proteases during the physiological state. This postulation may help explain in a relatively simple manner these two mutually exclusive phenomena, viz. the physiological endoproteolytic cleavage of $PrP^{C}$ and its pathological conversion into $PrP^{Sc}$.
© 2006 Elsevier Ltd. All rights reserved.

The prion protein exists as two isoforms: a cellular isoform ($PrP^{C}$) that is rich in α-helices, and a disease (scrapie) isoform $PrP^{Sc}$ that is rich in β-structures [1,2]. Many lines of evidence have predicated the persuasive argument that prions are composed largely, if not entirely, of the scrapie isoform [1]. After the synthesis of $PrP^{C}$, it is transited through the endoplasmic reticulum and Golgi apparatus to the cell surface where it is bound by a glycophosphatidyl inositol (GPI) anchor [3,4]. Subsequently, two mutually exclusive events take place – the metabolism of $PrP^{C}$ and the conversion of $PrP^{C}$ into $PrP^{Sc}$ [5–7].

During the physiological event, the initial degradation of $PrP^{C}$ involves endoproteolytic cleavage of

* Corresponding author. Tel.: +81 3 3351 6141x322; fax: +81 3 3351 6544.
*E-mail address:* k-kaneko@tokyo-med.ac.jp (K. Kaneko).

0306-9877/$ - see front matter © 2006 Elsevier Ltd. All rights reserved.
doi:10.1016/j.mehy.2006.07.038

the NH2-terminal fragment to produce a COOH-terminal polypeptide, which can be found in caveolae-like membrane domains or lipid rafts [5]. The NH2-terminal fragment of the PrP functions as a putative targeting element [8,9] and is essential for both its transport to the plasma membrane and the modulation of endocytosis [10]. A green fluorescent protein (GFP)-tagged version of $PrP^C$ has been observed to be properly anchored to the cell surface; its distribution pattern has been reported to be similar to that of the endogenous $PrP^C$, and it has shown labeling at the plasma membrane and in intracellular perinuclear compartments [11–17].

This cleavage site is mapped to the amino acid residues between the anti-PrP 3F4 and anti-PrP 13A5 epitopes (amino acid 108/111 to amino acid 138 in mouse PrP) [5,18,19] (Fig. 1). It has also been reported that $PrP^C$ cleavage occurs between amino acids 114 and 137 in chicken PrP [20] and between 110 and 113 in human PrP [21]. This proteolytic cleavage of $PrP^C$ in the brain is blocked by metalloprotease inhibitors [22].

Other investigators have reported that $PrP^C$ undergoes constitutive and phorbol ester-regulated cleavage. During such events, normal processing in human cells and murine neurons is upregulated by protein kinase C but not by protein kinase A [23]. Further experimentation indicated that a disintegrin and two metalloprotease family proteins, namely, ADAM10 and TACE, contribute to these cleavage reactions of $PrP^C$. ADAM10 contributes to the constitutive proteolytic cleavage of $PrP^C$, whereas TACE mainly participates in the regulated cleavage event [24].

The solution nuclear magnetic resonance (NMR) structure of monomeric recombinant $PrP^C$ illustrates that this region is largely unstructured [25–27], whereas the crystal structure of the human prion protein in dimer form and that of the sheep prion protein suggest that this region is, at least in part, structured and organized [28,29]. Apart from these results with recombinant PrP, little is known about the endogenous native $PrP^C$ conformation so far, except that these amino acid residues around the cleavage site have a hydrophobic property [30–32]; therefore, it is highly probable that they are buried within the native protein structure – a region that is barely accessible to the extrinsic proteases (Fig. 1) [33]. Thus, a putative molecular chaperone that should exhibit an unfolding activity on this hydrophobic region is expected to facilitate, at least to some extent, efficient $PrP^C$ proteolysis through its physiological metabolic pathway.

This assumption is reminiscent of the concept that the association of protein X in prion replication with the pathological condition that is unidentified thus far [26,34,35]. The binding of $PrP^C$ to protein X is accompanied by a conformational change (i.e., unfolding) in $PrP^C$, similar to that evident in the case of the molecular chaperone. This intermediate has been designated $PrP^*$ [36]. The $PrP^{Sc}$/$PrP^*$/protein X complex is modulated by an undefined process, following which $PrP^*$ is converted into $PrP^{Sc}$ and protein X is released [37]. Interestingly, a prion-like protein in yeast, namely Sup35, apparently requires intermediate levels of the molecular chaperone Hsp104 to undergo transformation to [$PSI^+$] [38].

It is noteworthy that the amino acid residues that are critical in terms of the target site of protein X for the pathological conversion into $PrP^{Sc}$ overlap at the physiological cleavage site where another putative molecular chaperone is expected to target and operate in conjunction with PrP proteases [2]. Hence, we can assume that these two putative molecules that exhibit a chaperone-like (i.e., unfolding) activity against the same hydrophobic residues in $PrP^C$ could be identical. If we assume that the converse is true, then protein X exists exclusively for the pathological condition in terms of prion replication; this, however, appears to be less probable. Instead, our current hypothesis may lend a satisfactory explanation for these two mutually exclusive phenomena, i.e., physiological endoproteolytic cleavage of $PrP^C$ and its pathological conversion into $PrP^{Sc}$. The identification of this putative molecular chaperone working in conjunction with proteases that target $PrP^C$ is significant

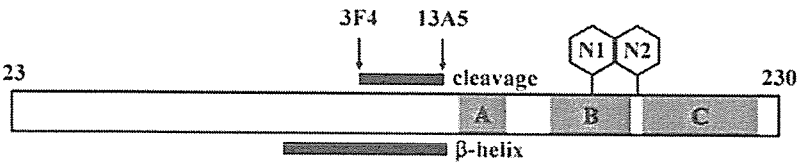


Figure 1 Endoproteolytic cleavage and pathological conversion into β-helix of the mouse cellular prion protein (Mo $PrP^C$). 3F4, anti-PrP 3F4 epitope (Mo 108/111); 13A5, anti-PrP13A5 epitope (Mo 138); A, helix A; B, helix B; C, helix C; N1 & N2, N-linked glycosylation sites (Mo 182/198); β-helix, β-helical region (Mo 90–140) of scrapie isoform of PrP ($PrP^{Sc}$); cleavage, mapped region of $PrP^C$ cleavage site.

because it could also be also directed toward identifying protein X in prion replication – an issue that has not been elucidated for over a decade.

## References


[1] Prusiner SB. Prions Proc Natl Acad Sci USA 1998;95: 13363–83.

[2] Wille H, Michelitsch MD, Guenebaut V, et al. Structural studies of the scrapie prion protein by electron crystallography. Proc Natl Acad Sci USA 2002;99:3563–8.

[3] Stahl N, Borchelt DR, Hsiao K, Prusiner SB. Scrapie prion protein contains a phosphatidylinositol glycolipid. Cell 1987;51:229–40.

[4] Caughey B, Race RE, Ernst D, Buchmeier MJ, Chesebro B. Prion protein biosynthesis in scrapie-infected and uninfected neuroblastoma cells. J Virol 1989;63:175–81.

[5] Taraboulos A, Scott M, Semenov A, et al. Cholesterol depletion and modification of COOH-terminal targeting sequence of the prion protein inhibit formation of the scrapie isoform. J Cell Biol 1995;129:121–32.

[6] Vey M, Pilkuhn S, Wille H, et al. Subcellular colocalization of the cellular and scrapie prion proteins in caveolae-like membranous domains. Proc Natl Acad Sci USA 1996;93: 14945–9.

[7] Kaneko K, Vey M, Scott M, et al. COOH-terminal sequence of the cellular prion protein directs subcellular trafficking and controls conversion into the scrapie isoform. Proc Natl Acad Sci USA 1997;94:2333–8.

[8] Shyng SL, Heuser JE, Harris DA. A glycolipid-anchored prion protein is endocytosed via clathrin-coated pits. J Cell Biol 1994;125:1239–50.

[9] Shyng SL, Moulder KL, Lesko A, Harris DA. The N-terminal domain of a glycolipid-anchored prion protein is essential for its endocytosis via clathrin-coated pits. J Biol Chem 1995;270:14793–800.

[10] Nunziante M, Gilch S, Schatzl HM. Essential role of the prion protein N terminus in subcellular trafficking and half-life of cellular prion protein. J Biol Chem 2003;278:3726–34.

[11] Lee KS, Magalhaes AC, Zanata SM, et al. Internalization of mammalian fluorescent cellular prion protein and N-terminal deletion mutants in living cells. J Neurochem 2001;79:79–87.

[12] Magalhaes AC, Silva JA, Lee KS, et al. Endocytic intermediates involved with the intracellular trafficking of a fluorescent cellular prion protein. J Biol Chem 2002;277: 33311–8.

[13] Negro A, Ballarin C, Bertoli A, Massimino ML, Sorgato MC. The metabolism and imaging in live cells of the bovine prion protein in its native form or carrying single amino acid substitutions. Mol Cell Neurosci 2001;17:521–38.

[14] Lorenz H, Windl O, Kretzschmar HA. Cellular phenotyping of secretory and nuclear prion proteins associated with inherited prion diseases. J Biol Chem 2002;277: 8508–16.

[15] Ivanova L, Barmada S, Kummer T, Harris DA. Mutant prion proteins are partially retained in the endoplasmic reticulum. J Biol Chem 2001;276:42409–21.

[16] Hachiya NS, Watanabe K, Sakasegawa Y, Kaneko K. Microtubules-associated intracellular localization of the NH(2)-terminal cellular prion protein fragment. Biochem Biophys Res Commun 2004;313:818–23.

[17] Hachiya NS, Watanabe K, Yamada M, Sakasegawa Y, Kaneko K. Anterograde and retrograde intracellular trafficking of fluorescent cellular prion protein. Biochem Biophys Res Commun 2004;315:802–7.

[18] Rogers M, Serban D, Gyuris T, et al. Epitope mapping of the Syrian hamster prion protein utilizing chimeric and mutant genes in a vaccinia virus expression system. J Immunol 1991;147:3568–74.

[19] Pan KM, Stahl N, Prusiner SB. Purification and properties of the cellular prion protein from Syrian hamster brain. Protein Sci 1992;1:1343–52.

[20] Harris DA, Huber MT, van Dijken P, et al. Processing of a cellular prion protein: identification of N- and C-terminal cleavage sites. Biochemistry 1993;32:1009–10016.

[21] Chen SG, Teplow DB, Parchi P, et al. Truncated forms of the human prion protein in normal brain and in prion diseases. J Biol Chem 1995;270:19173–80.

[22] Jimenez-Huete A, Lievens PM, Vidal R, et al. Endogenous proteolytic cleavage of normal and disease-associated isoforms of the human prion protein in neural and non-neural tissues. Am J Pathol 1998;153: 1561–72.

[23] Vincent B, Paitel E, Frobert Y, et al. Phorbol ester-regulated cleavage of normal prion protein in HEK293 human cells and murine neurons. J Biol Chem 2000;275:35612–6.

[24] Vincent B, Paitel E, Saftig P, et al. The disintegrins ADAM10 and TACE contribute to the constitutive and phorbol ester-regulated normal cleavage of the cellular prion protein. J Biol Chem 2001;276:37743–6.

[25] Donne DG, Viles JH, Groth D, et al. Structure of the recombinant full-length hamster prion protein PrP(29–231): the N terminus is highly flexible. Proc Natl Acad Sci USA 1997;94:13452–7.

[26] James TL, Liu H, Ulyanov NB, et al. Solution structure of a 142-residue recombinant prion protein corresponding to the infectious fragment of the scrapie isoform. Proc Natl Acad Sci USA 1997;94:10086–91.

[27] Zahn R, Liu A, Luhrs T, et al. NMR solution structure of the human prion protein. Proc Natl Acad Sci USA 2000;97:145–50.

[28] Knaus KJ, Morillas M, Swietnicki W, et al. Crystal structure of the human prion protein reveals a mechanism for oligomerization. Nat Struct Biol 2001;8:770–4.

[29] Haire LF, Whyte SM, Vasisht N, et al. The crystal structure of the globular domain of sheep prion protein. J Mol Biol 2004;336:1175–83.

[30] Pillot T, Lins L, Goethals M, et al. The 118–135 peptide of the human prion protein forms amyloid fibrils and induces liposome fusion. J Mol Biol 1997;274:381–93.

[31] Jobling MF, Stewart LR, White AR, et al. The hydrophobic core sequence modulates the neurotoxic and secondary structure properties of the prion peptide 106–126. J Neurochem 1999;73:1557–65.

[32] Saez-Cirion A, Nieva JL, Gallaher WR. The hydrophobic internal region of bovine prion protein shares structural and functional properties with HIV type 1 fusion peptide. AIDS Res Hum Retroviruses 2003;19:969–78.

[33] Kaneko K, Hachiya NS. The alternative role of 14-3-3 zeta as a sweeper of misfolded proteins in disease conditions. Med Hypotheses 2006;67:169–71.

[34] Telling GC, Scott M, Mastrianni J, et al. Prion propagation in mice expressing human and chimeric PrP transgenes implicates the interaction of cellular PrP with another protein. Cell 1995;83:79–90.

[35] Kaneko K, Zulianello L, Scott M, et al. Evidence for protein X binding to a discontinuous epitope on the cellular prion protein during scrapie prion propagation. Proc Natl Acad Sci USA 1997;94:10069–74.

[36] Cohen FE, Prusiner SB. Pathologic conformations of prion proteins. Annu Rev Biochem 1998;67:793–819.
[37] Prusiner SB, Scott MR, DeArmond SJ, Cohen FE. Prion protein biology. Cell 1998;93:337–48.
[38] Chernoff YO, Lindquist SL, Ono B, Inge-Vechtomov SG, Liebman SW. Role of the chaperone protein Hsp104 in propagation of the yeast prion-like factor [*psi*⁻]. Science 1995;268:880–4.

Available online at www.sciencedirect.com
ScienceDirect

Available online at www.sciencedirect.com
SCIENCE DIRECT®
Neuroscience Letters 402 (2006) 222–226
Neuroscience Letters
www.elsevier.com/locate/neulet

# Intracerebroventricular delivery of dominant negative prion protein in a mouse model of iatrogenic Creutzfeldt-Jakob disease after dura graft transplantation

Kazuhide Furuya[a,*], Nobutaka Kawahara[a], Yoshio Yamakawa[b], Hitaru Kishida[c], Naomi S. Hachiya[d], Masahiro Nishijima[b], Takaaki Kirino[a], Kiyotoshi Kaneko[d]

[a] *Department of Neurosurgery, Faculty of Medicine, University of Tokyo, 7-3-1 Hongo, Bunkyo-ku, Tokyo 113-8655, Japan*
[b] *Department of Biochemistry and Cell Biology, National Institute of Infectious Diseases, Shinjuku-ku, Tokyo 162-8640, Japan*
[c] *Department of Neurology, Yokohama City University, Yokohama 236-0004, Japan*
[d] *Second Department of Physiology, Tokyo Medical University, Shinjuku-ku, Tokyo 160-8402, Japan*

Received 21 February 2006; received in revised form 10 March 2006; accepted 25 March 2006

**Abstract**

We have developed a novel procedure in which a small collagen sheet (3 mm × 3 mm) absorbing prion-infected brain homogenates was transplanted onto the brain surface of highly prion-susceptible transgenic mice (Tg(MoPrP)4053/FVB), as an animal model of iatrogenic Creutzfeldt-Jakob disease (iCJD) caused by prion-contaminated cadaveric dura graft transplantation. Using the iCJD model, we further investigated the in vivo efficacy of dominant negative recombinant prion protein with lysine substitution at mouse codon 218 (rPrP-Q218K), which is known to inhibit prion replication in vitro (H. Kishida, Y. Sakasegawa, K. Watanabe, Y. Yamakawa, M. Nishijima, Y. Kuroiwa, N.S. Hachiya, K. Kaneko, Non-glycosylphosphatidylinositol (GPI)-anchored recombinant prion protein with dominant-negative mutation inhibits PrPSc replication in vitro, Amyloid, vol. 11, 2004, pp. 14–20.). Following 7-day intracerebroventricular administration of the rPrP-Q218K via an indwelling catheter connected to the implanted osmotic pump, the median incubation period of Tg(MoPrP)4053/FVB was prolonged considerably from 117 days to 131 days ($p = 0.016$, log-rank test) in the rPrP-Q218K-treated group, even after a lengthy latency period of as long as 30 days by starting the rPrP-Q218K injection. Whether wild-type rPrP, other mutant rPrPs, or the combination of rPrP-Q218K with other anti-prion compounds might extend the survival period in that condition must be further investigated.
© 2006 Elsevier Ireland Ltd. All rights reserved.

*Keywords:* Iatrogenic Creutzfeldt-Jakob disease (iCJD); Animal model of iCJD; Osmotic pump; Highly prion-susceptible transgenic mice (Tg(MoPrP)4053/FVB); Dominant negative recombinant prion protein (rPrP-Q218K)

Prion diseases are a group of neurodegenerative disorders including kuru, Creutzfeldt-Jakob disease (CJD), Gerstmann-Sträussler-Scheinker disease (GSS), and fatal familial insomnia (FFI) in humans, scrapie in sheep, and bovine spongiform encephalopathy (BSE) in cattle, which comprise sporadic, genetic, or infectious disorders [22]. The post-translational conformational change of the cellular isoform of prion protein ($PrP^C$) into the scrapie isoform of prion protein ($PrP^{Sc}$) is the fundamental process underlying the pathogenesis of prion diseases [23,24].

Among the infectious forms of CJD, iatrogenic CJD (iCJD) is the most representative. In that form, several sources for the iatrogenic prion infection have been reported, including improperly sterilized cortical and depth electrodes, transplanted corneas, cadaveric pituitary-derived human growth hormone/gonadtropin, and dura graft [4]. By the year 2000, 114 cases of iCJD caused by cadaveric dura transplants from CJD patients had been reported worldwide [4]; about two-thirds of the CJD patients who had received cadaveric dura graft transplantation were from Japan [6,12]. That highest incidence in Japan most probably results from extensive use of cadaveric dura graft: it far exceeds the use in any other country [2]. Emerging patients as well as suspected cases, and the increase in the mean and range of the latency period all suggest that this outbreak is ongoing [3]. In spite of its significance and urgent necessity, no

* Corresponding author. Tel.: +81 3 5800 8853; fax: +81 3 5800 8655.
*E-mail address:* furuya-nsu@umin.ac.jp (K. Furuya).

0304-3940/$ – see front matter © 2006 Elsevier Ireland Ltd. All rights reserved.
doi:10.1016/j.neulet.2006.03.062

animal model with prion transmission via cortico-dural interface has been verified so far. Consequently, development of an animal model toward exploration of prophylactic and therapeutic approaches is urgent.

Naturally occurring polymorphic PrP variants (Q171R and E219K) are known to render sheep and humans resistant to scrapie and CJD, respectively, and were found to act as dominant negatives [13,33]. Similarly, recombinant mouse PrP with a lysine variant at codon 218 (rPrP-Q218K) corresponding to human E219K, but not wild-type rPrP, exclusively inhibited prion replication as dominant negatives in scrapie-infected mouse neuro2a (ScN2a) cells without reducing cell viability in vitro [13].

With this background, we have developed a mouse model of iCJD after artificial dura graft transplantation. Having established the mouse model for the first time in vivo, we further investigated whether the dominant negative rPrP-Q218K can be protective against experimental iCJD after prion-contaminated dura graft transplantation in vivo.

Transgenic mice with FVB background harboring a high-copy-number of wild-type PrP-A transgenes (Tg(MoPrP-A)B4053/FVB) [32] were kindly supplied by Dr. S.B. Prusiner of UCSF. A mouse-adapted scrapie Obihiro strain [29], a kind gift from Dr. M. Horiuchi of Hokkaido University, was inoculated intracerebrally into the Tg(MoPrP-A)B4053/FVB. Their brains were collected approximately 70 days after inoculation, and 10% (w/v) brain homogenates in phosphate buffer saline (PBS) were prepared and further provided as inocula (30 μl each) using a 27-gauge disposable hypodermic needle inserted into the right parietal lobe. Diagnosis of scrapie in the transgenic mice has been described extensively elsewhere [5,25]. Beginning 50 days after inoculation, the mice and hamsters were examined every 3 days for neurologic dysfunction. Once clinical signs were detected, the animals were inspected daily and sacrificed when death was imminent. Representative fractions of brains were removed for histological analyses to confirm the scrapie diagnosis.

The recombinant PrP (rPrP) was expressed as inclusion bodies in the *E. coli* BL21 (DE3) (Stratagene, La Jolla, CA) in the presence of 0.1 mM isopropyl-β-D-thiogalactopyranoside (IPTG). Inclusion bodies were collected from sonicated lysates by centrifugation at 27,000 × *g* for 10 min, washed three times in Buffer A (2 M urea, 25 mM Tris–HCl, pH 7.5, 150 mM NaCl, 2 mM β-mercaptoethanol (β-ME), 0.5 mM phenylmethylsulfonyl fluoride (PMSF)), and solubilized in Buffer B (8 M urea, 25 mM Tris–HCl, pH 7.5, 2 mM β-ME, 0.5 mM PMSF). After centrifugation (200,000 × *g*, 30 min), the supernatant was applied to a CM-Sepharose column (Amersham Biosciences Corp., Piscataway, NJ), washed with Buffer B containing 100 mM NaCl and eluted with Buffer B containing 150 mM NaCl. The eluate containing rPrP was applied to a Ni-NTA agarose column (Qiagen Inc., Valencia, CA), washed with Buffer B containing 5 mM imidazol and eluted with Buffer B containing 200 mM imidazol. The eluate was diluted 10-fold in 1 M arginine-HCl, pH 8.0, 1 mM reduced glutathione, 0.8 mM oxidized glutathione and incubated at 4 °C overnight. After incubation at 37 °C for 10 min, the refolded recombinant proteins were concentrated and buffer-changed into PBS using ultrafiltration (Ultrafree-15 centrifugal filter device-Biomax 10 K NMWL membrane; Millipore Co., Bedford, MA). Concentrations of rPrP were calculated by absorbance at 280 nm with a specific absorbance unit of 2.70 [15].

As an animal model of iCJD after prion-contaminated dura graft transplantation, the Tg(MoPrP-A)B4053 mice were anesthetized with ketamine and xylazine. Subsequently, the head of each was fixed to a stereotaxic frame. Following a 4 mm × 4 mm craniectomy on the right skull, a small collagen sheet (3 mm × 3 mm) absorbing either 5 μl of 10% brain homogenates derived from prion-infected mice ($n = 16$) or PBS ($n = 12$) as a control was transplanted on the brain surface of Tg(MoPrP-A)B4053 ($n = 5$ each). All procedures in animals accorded strictly with guidelines for experiments involving experimental animals performed at the National Institute of Infectious Diseases, Japan. These mice were re-anesthetized followed by implantation of osmotic pumps (200 μl, Alzet 2001; Alza Corp., Palo Alto, CA) in the back. The pumps were filled with either 200 μg/ml of rPrP-Q218K at 30 ($n = 7$) or 60 ($n = 9$) days after prion-contaminated dura graft transplantation or PBS ($n = 6$ each). These solutions were then administered intracerebroventricularly via an indwelling catheter connected to the pump at a rate of 1 μ/h for 7 days.

Brain tissue was homogenized in 50 mM Tris–HCl buffer (pH 7.5) containing 0.1 M NaCl (TN-buffer) to 10% (w/v) with Multi-beads Shocker (Yasui Kikai Corp., Tokyo). The homogenate (250 μl, containing 25 mg brain tissue equivalent) was clarified by the addition of equal volume of detergent buffer (TN-buffer containing 4% zwittergent 3-13 and 1% sarkosyl) and 25 μl of 2-butanol. After extensive sonication, the mixture was simultaneously digested with collagenase (250 μg) and DNase I (20 μg) at 37 °C for 30 min. Thereafter, 20 μg of proteinase K (PK) was added to the reaction mixture and incubated for 30 min; $PrP^{Sc}$ was then precipitated by addition of 250 μl of 5:1 mixture of 2-butanol and methanol containing 3 mM phenylmethylsulfonyl fluoride. The precipitates collected by centrifugation at 15,000 rpm for 10 min were dissolved in 100 μl of SDS-PAGE sampling buffer and heated at 100 °C for 5 min.

Five micrograms of total brain homogenates in 10 μl from mice in 30 ($n = 3$), 60 ($n = 3$), 90 ($n = 3$), and 120 ($n = 2$) days after prion-contaminated dura graft transplantation was electrophoresed in 12% polyacrylamide gel (NuPAGE Bis–Tris gel, Invitrogen, Carlsbad, CA) for 60 min at a constant voltage of 200 V. Then, total proteins were transferred onto PVDF membrane at a constant voltage of 25 V for 45 min. Mouse $PrP^{Sc}$ was reacted with a rabbit polyclonal anti-mouse PrP antibody P-8, which was purified from the rabbit serum immunized with the synthetic peptide with mouse PrP residues 94–108 (THNQWN KPSKPKTNML). Next, HRP-linked anti-rabbit IgG (Amersham Biosciences, Uppsala, Sweden) was used as a secondary antibody. Immunoreactivity was detected with an enhanced chemiluminescence kit (ECL; Amersham Biosciences, Uppsala, Sweden) and visualized on autoradiographic film.

Brain tissues ($n = 3$ in 120-day group) were fixed with 10% buffered-formalin for 48–72 h. Mouse $PrP^{Sc}$ was first inacti-

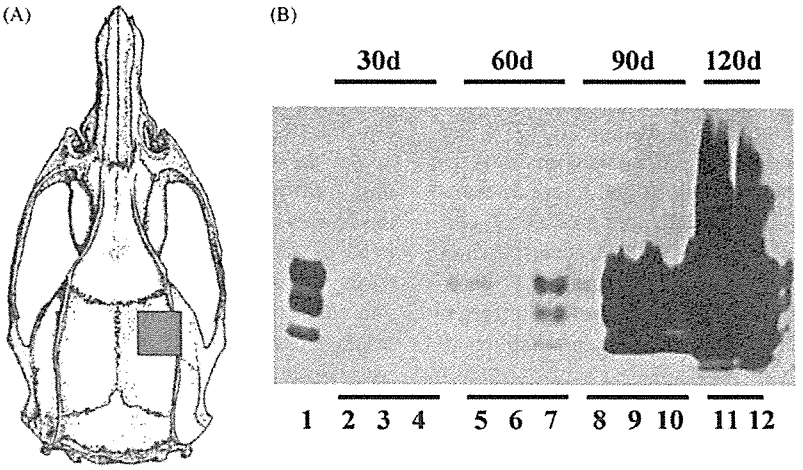


Fig. 1. A mouse model of iatrogenic Creutzfeldt-Jakob disease (iCJD) after prion-contaminated dura graft transplantation. (A) A small collagen sheet (3 mm × 3 mm) containing brain homogenates derived from prion-infected mice was transplanted on the brain surface of highly prion-susceptible transgenic mice (Tg(MoPrP-A)B4053, hatched area). (B) Western blot analyses of Tg(MoPrP-A)B4053 brains at 30, 60, 90 and 120 days (three brains each) after transplantation. Initial detection of $PrP^{Sc}$ in two-thirds of the animals at 60 days (lanes 5, 6 and 7) and strong detection at 90 (lanes 8, 9 and 10) and 120 days (lanes 11 and 12) are observed in a time-dependent manner. Lane 1: Brain homogenates from pooled prion-infected mice as a positive control.

vated by immersing tissues into 98% formic acid for 1 h at room temperature. Samples were re-fixed with the formalin overnight, dehydrated in graded ethanol, and cleared in xylene; then they were embedded in paraffin. Sections cut at 3 μm thickness were mounted on silane-coated slide glasses. After deparaffinization, sections were stained with hematoxylin and eosin. For immunostaining, the deparaffinized sections were autoclaved at 121 °C for 20 min in the presence of 1 mM HCl to destroy $PrP^{C}$ [19]; endogenous peroxidase activity was blocked by 0.3% hydrogen peroxide for 5 min at room temperature. The sections were treated with 10% normal goat serum in PBS for 5 min. Then they were reacted for 30 min with anti-PrP polyclonal antibody (Ab221–236) [31], which is a rabbit polyclonal anti-bovine PrP purified from the rabbit serum immunized with the synthetic peptide with bovine PrP residues 221–240 (VEQMCITQYQRESQAYYQRG), but cross-reacts with mouse $PrP^{C}$. The HRP-labeled polymer method (Envision + kit; Dako Cytomation, Carpinteria, CA) was used according to the manufacturer's instructions. Signals were detected using diaminobenzidine (DAB).

The (Tg(MoPrP-A)B4053 harboring a high-copy-number of wild-type PrP-A transgenes were highly susceptible to mouse prions; they exhibited an abbreviated scrapie incubation time of about 45 days after intracerebral inoculation, which is consistent with a previous observation [32]. To establish a mouse model of iCJD after prion-contaminated dura graft transplantation, a small collagen sheet bearing 5 μl of 10% prion-infected mouse brain homogenates was transplanted on the brain surface of Tg(MoPrP-A)B4053 (Fig. 1A). Consequently, all animals died approximately 120 days after the

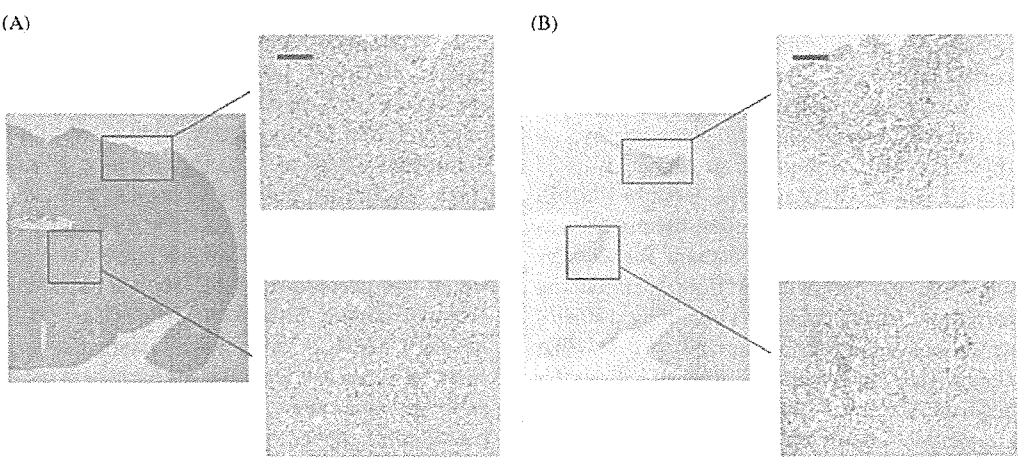


Fig. 2. Accumulation of mouse $PrP^{Sc}$ in brains from the iCJD model at 120 days after prion-contaminated dura graft transplantation revealed by light microscopy and immunohistochemstry. Representative brain sections stained with either hematoxylin or eosin in panel A, or immunostained with anti-PrP antibody (Ab221–236) in panel B. Scale bars = 100 μm.